



HAL
open science

Multiscale examination of deformation and fracture mechanisms of a duplex advanced high strength steel: Effect of testing temperature and of micromechanical interactions between microstructural constituents

Anne-Françoise Gourgues-Lorenzon, Q. Tonizzo, Daniel Caillard, A. Perlade, M. Mazière, A.F. Gourgues-Lorenzon

► To cite this version:

Anne-Françoise Gourgues-Lorenzon, Q. Tonizzo, Daniel Caillard, A. Perlade, M. Mazière, et al.. Multiscale examination of deformation and fracture mechanisms of a duplex advanced high strength steel: Effect of testing temperature and of micromechanical interactions between microstructural constituents. *Materials Science and Engineering: A*, 2019, 764, pp.138196. 10.1016/j.msea.2019.138196 . hal-03065259

HAL Id: hal-03065259

<https://hal.science/hal-03065259>

Submitted on 21 Dec 2021

HAL is a multi-disciplinary open access archive for the deposit and dissemination of scientific research documents, whether they are published or not. The documents may come from teaching and research institutions in France or abroad, or from public or private research centers.

L'archive ouverte pluridisciplinaire **HAL**, est destinée au dépôt et à la diffusion de documents scientifiques de niveau recherche, publiés ou non, émanant des établissements d'enseignement et de recherche français ou étrangers, des laboratoires publics ou privés.



Distributed under a Creative Commons Attribution - NonCommercial 4.0 International License

Emissivity measurement of tungsten plasma facing components of the WEST tokamak

J. Gaspar^a, C. Pocheau^b, Y. Corre^b, N. Ehret^a, D. Guilhem^b, M. Houry^b, T. Loarer^b, Th. Loewenhoff^c, C. Martin^d, C. Pardanaud^d, G. Pintsuk^c, M. Richou^b, F. Rigollet^a, H. Roche^b, G. Sepulcre^b and M. Wirtz^c

^a Aix Marseille Univ, CNRS, IUSTI, Marseille, France

^b CEA Cadarache, F-13108 St Paul lez Durance, France

^c Forschungszentrum Jülich, Institut für Energie- und Klimaforschung, 52425 Jülich, Germany

^d Aix Marseille Univ, CNRS, PIIM, Marseille, France

Corresponding author email address: jonathan.gaspar@univ-amu.fr

Abstract. Since tungsten (W) has been selected as material for the ITER divertor target the knowledge of the emissivity in the infrared (IR) wavelength range becomes mandatory. A dedicated setup has been developed to measure the emissivity in the wavelength range 1.7 - 4.75 μm and the temperature domain 200 - 850 $^{\circ}\text{C}$. The paper presents the emissivity measurements on W samples coming from actively cooled bulk W components (ITER-like) and W-coated graphite component of the WEST divertor. W samples with damaged surfaces generated by transient heat load as those observed in fusion machines, including micro-cracks and crack network, are also investigated. The dependence on wavelength, temperature and surface state are shown and discussed.

1. Introduction

The objective of controlled fusion is to recover the energy produced by fusion reactions and convert it into usable energy forms. One key factor in the success of fusion facilities will be the ability of its plasma facing components (PFCs) to handle high heat fluxes as expected in the ITER divertor region, up to 10 MW/m² in steady state and 20 MW/m² in slow transient [1-3]. The WEST tokamak provides an integrated platform for testing the ITER divertor components under relevant power loads, particle fluence and time scales [4, 5] in a full metallic environment. Plasma experiences performed in WEST will also allow validating the PFC protection strategy in a full metallic environment based on infrared (IR) thermography [6-8]. The most accurate surface temperature measurement is therefore mandatory and required for both machine protection and physics studies. Over the IR detection wavelength range of 1.7-4.75 μm , the tungsten emissivity is expected to be in a range of 0.05-0.5. Compared to previous configuration using carbon as PFC, with high and rather constant emissivity values of 0.7-0.8, the huge potential variation of the tungsten emissivity by a factor of 10 has to be very carefully assessed. It is also worth mentioning that for low emissivity values, the reflected fluxes can significantly contribute to the collected signal by the IR system and this has to be considered in the IR monitoring system. As a consequence, with the introduction of all-metal walls in fusion devices [9, 10], surface emissivity becomes a very important and challenging issue for accurate surface temperature measurement [11, 12].

Tungsten and its emissivity have been studied from the beginning of the 20th century [13-18] up to now [19-25]. All these studies have been performed on different kinds of samples depending on manufacturing process (roughness, grade...) and for different ranges of temperatures and wavelengths not always relevant for a direct use in fusion devices. However, these studies show that the emissivity exhibit strong dependences with wavelength, temperature and surface state (roughness, cracks, pollution). Also, for the same wavelength and temperature a large spread of tungsten emissivity depending on the manufacturing process (mainly from 0.05 to 0.5) result. The theoretical models

developed for the emissivity and reflectivity of the tungsten are valid for optical smooth surfaces which is not the case for all the PFCs installed in the WEST divertor presenting non-negligible roughness ($R_a > 1\mu\text{m}$). In addition, all along plasma operations, the surface roughness of more or less all the PFCs will be modified through plasma surface interaction leading to erosion, deposition and possible damages (local melting...). In this context, a dedicated setup has been developed at CEA/IRFM to measure the emissivity of W samples coming from actively cooled bulk W components (also called ITER-like PFU [4]) and W-coated graphite component of the WEST divertor used in the early phase experiment [26, 27]. The principle of the measurement and the experimental setup are depicted in section 2. The W samples selected here are presented in section 3, including polished, unpolished and pre-damaged surfaces performed in High Heat Flux (HHF) facility (electron beam). Emissivity measurements are presented and discussed in section 4.

2. Experimental setup

Figure 1 shows the experimental setup developed at CEA/IRFM for emissivity measurement. A sample holder is located inside a vacuum vessel (diameter 350 mm). The high vacuum (about 10^{-5} Pa) used is required to prevent any pollution of the sample, such as oxidation. The sample is heated at its back by a radiant and electron bombardment heater of 9 mm diameter. With this system a W sample of $12 \times 18 \times 3 \text{ mm}^3$ can be typically heated up to $850 \text{ }^\circ\text{C}$. The vacuum vessel is closed with a sapphire window allowing the measurement of the sample top surface by IR thermography in the studied wavelength range of $1.7\text{-}4.75 \mu\text{m}$. The IR camera is a ‘‘CEDIP’’ camera with 320×256 pixels, InSb detectors sensitive in the $1\text{-}5 \mu\text{m}$ wavelength range and equipped with a filter holder. The IR camera is actively cooled with a cooling bath in order to keep the same temperature as the one used for the calibration performed for each filter used in this study with the sapphire window placed in the optical path and same optics. Multiple screens are installed in this setup. The one outside the vacuum chamber is placed in front the IR camera to avoid heating and track the possible offset drift of the camera during the campaign. Since low emissivities are expected, the contribution of the potential reflected fluxes should be inhibited in this set up. The screen inside the vacuum vessel, in blue on figure 1, allows for avoiding reflection on the top surface of the sample coming from the hot sample holder after multiple reflections inside the vacuum vessel. The multiple reflections have been highlighted by measuring a highly reflective silver sample changing from apparent emissivity of about 0.2 to 0.02-0.03 (close to expected values), without and with the screen respectively. The sample temperature is measured by a type K ThermoCouple (TC errors of $1.5 \text{ }^\circ\text{C}$ for $T < 375 \text{ }^\circ\text{C}$ and 0.4% for $T > 375 \text{ }^\circ\text{C}$) installed in the samples with a 1.1mm hole filled with graphite adhesive ensuring a good thermal contact between the thermocouple and the sample

The emissivity, $\varepsilon(\lambda, T)$ is defined as the ratio between the radiation emitted by the surface $L(\lambda, T)$ and the radiation emitted by a black body at the same temperature $L^0(\lambda, T)$ as follows:

$$\varepsilon(\lambda, T) = \frac{L(\lambda, T)}{L^0(\lambda, T)} \quad (1)$$

In our experimental setup the radiance emitted by the surface $L(\lambda, T)$ is measured by the IR camera, equipped with a filter and calibrated with a black body source. Then the radiation emitted by the surface of the sample assuming black body emission is calculated with the Planck formula with the temperature measured by the TC and integrated in the wavelength range of the filter as follows:

$$L^0(\lambda, T) = \int_{\lambda} F(\lambda) \frac{c_1 \lambda^{-5}}{\exp\left(\frac{c_2}{\lambda T_{TC}}\right) - 1} d\lambda \quad (2)$$

Where $F(\lambda)$ being the filter spectral transmittance, λ the wavelength, T_{TC} the temperature measured by the thermocouple expressed in K, $C_1 = 2hc \approx 1.19 \times 10^{-16} \frac{W}{m^2 \cdot sr}$ and $C_2 = \frac{hc}{k_B} \approx 1.44 \times 10^{-2} m \cdot K$ the radiation constants.

The emissivity measured is the integrated emissivity in the filter wavelength range. For this study we used seven narrow filters centered from 1.7 to 4.75 μm and one large band filter between 1.6 and 2.1 μm . The spectral transmissions of each filter have been measured in the range from 1 to 25 μm by a spectrometer. Three of these filters are installed in WEST (experimental campaigns 2017 and 2018), the large band filter corresponds to the one used by the Very High spatial Resolution (VHR) [28] view. The narrow filters at 3.9 and 4.35 μm correspond to the STanDard (STD) and the Wide Angle (WA) views, respectively [6]. The seven narrow filters are $1.7 \pm 0.1 \mu m$, $2.14 \pm 0.05 \mu m$, $2.6 \pm 0.05 \mu m$, $3.255 \pm 0.05 \mu m$, $3.9 \pm 0.1 \mu m$, $4.35 \pm 0.1 \mu m$ and $4.75 \pm 0.075 \mu m$.

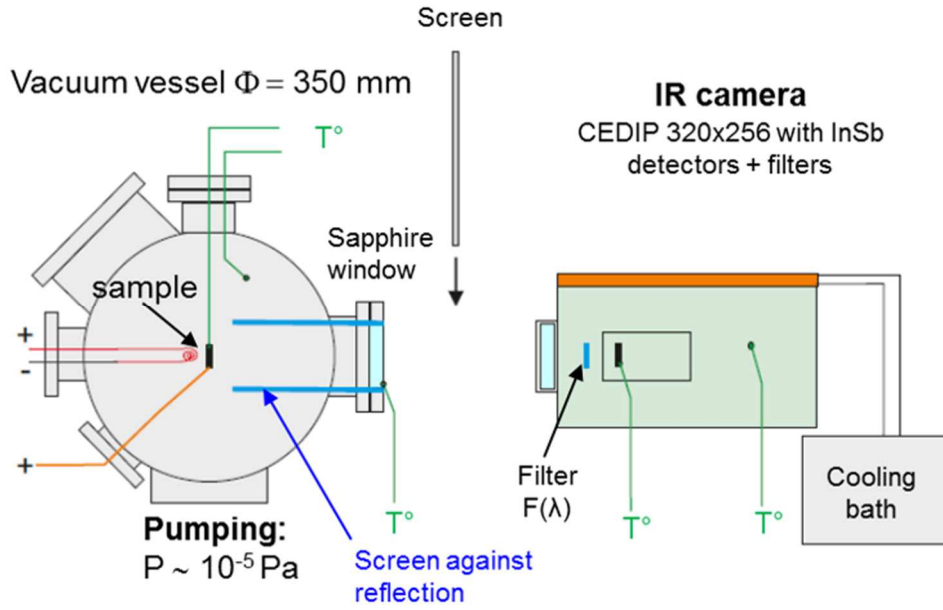


Figure 1. Schematic view of the experimental setup: IR camera, cooling bath, vacuum vessel, screen against reflection.

3. Samples

Figure 2 shows the 4 samples used in this study. The so-called “W bulk” is a sample sliced from a W bloc manufactured with the same specifications (roughness R_a , grain size and orientation in the heat flux orientation from the top surface to the cooling tube) as the ITER-like PFC installed in the WEST divertor. The top surface has the same roughness, $R_a=1.12 \mu m$, than the ITER-like PFC in WEST. The W-coated graphite sample was sliced from a W-coated graphite divertor PFC (graphite grade R 6710) which was tested in a HHF experiment (20 cycles of $8 MWm^2$ for 2 s). The coating thickness is about $12 \mu m$ [26,27] with $R_a = 2 \mu m$. The two other samples (damage #1 and #2) have been provided by the same manufacturer as the W bulk sample. After cutting they have been polished, from $R_a = 1.2$ to $0.1 \mu m$ and exposed to HHF loads (10^5 transient pulses performed in the electron beam facility JUDITH 2 [29]) in order to mimic long term damages produced by plasma exposure. The induced heat load damage procedure is based on a steady state heat loading at $700^\circ C$ and 10^5 short transients (0.48 ms) with different intensity level. Heat impact factors of 3 and $6 MW/m^2s^{0.5}$ were applied on damage #1

and #2 samples, respectively. The roughness increased up to 0.42 and 1.39 μm by the appearance of micro-cracks and crack networks for damage samples #1 and #2, respectively.

Furthermore, these two kinds of damage have been reproduced on purpose on a dedicated ITER-like component currently installed in the WEST tokamak divertor. The goal of this experiment is to study damage evolution (crack evolution) and PFC ageing under plasma exposure. The pre-damaged component is monitored by the VHR IR system with spatial resolution of 0.1 mm/pixel [28]. Note also that the undamaged part of sample was used to get a measurement on a polished surface.

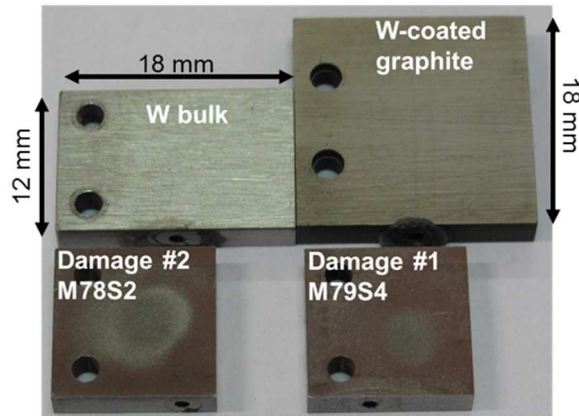


Figure 2. W samples selected for WEST early phase experiments

Figure 3 shows typical IR images at 250 °C of the four samples studied here, the region of interest (circles) used for the emissivity measurement appear in the figures. In the W bulk and coating cases, the IR emissions of the surface are quite uniform. The measurements are performed over the circle of 7mm diameter indicated in dashed line on the figure. In contrast, the damaged samples have strong variation of the IR emissions on the surface from the polished to the damaged area. The area of measurement has been reduced for these samples to 1.5 mm diameter corresponding to the half width of the electron beam size used to induce the damages. The same region of interest has been used for the two samples and the polished area for the following results.

For each emissivity measurement an interval of confidence will be displayed. These intervals of confidences are determined with the standard deviation of the digital level measured in the region of interest used for the measurements and the thermocouple accuracy given by the manufacturer.

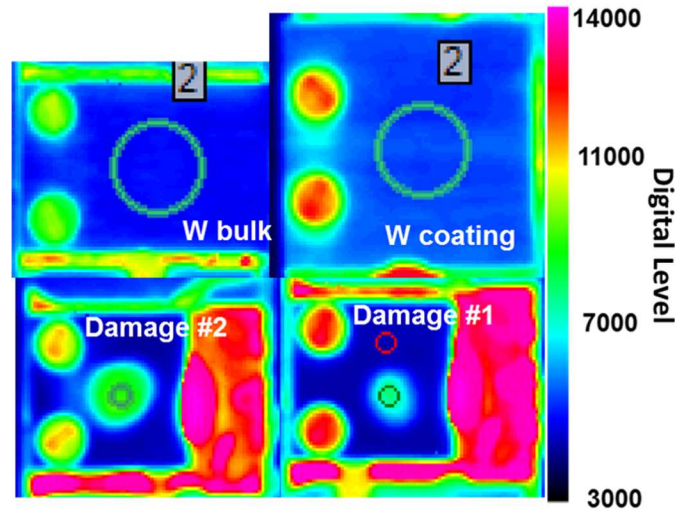


Figure 3. IR image illustration of the 4 samples at 250 °C and 3.9 μm : (top left) W bulk (top right) W coating (bottom left) W damaged samples with crack network and (bottom right) W damaged samples with cracks.

4. Experimental results

4.1. W bulk

Figures 4 and 5 show the W bulk emissivity dependences with the temperature and wavelength respectively. As expected from the literature [16], the overall trend of the measured emissivity exhibits an increase with the temperature and a drop with the wavelength. The strongest dependence is on the wavelength with a factor three (~ 0.3 to 0.1 roughly) for the emissivity at $1.7 \mu\text{m}$ in comparison to $4.75 \mu\text{m}$. The temperature dependence is almost linear over the studied temperature range with an increase of 0.04 between 200 and $800 \text{ }^\circ\text{C}$ for all the samples. This behavior leads to higher influence at high wavelength as for the STD and WA filters contrary to low wavelength as for the VHR filter. As expected, the measured emissivity with the VHR large band filter ($1.6\text{-}2.1 \mu\text{m}$) is between the measurements with the narrow filters at 1.7 and $2.14 \mu\text{m}$. One can note that the theoretical model proposed by Hagen-Rubens [30], not displayed here, describes well the temperature dependence of the measured emissivity, increase of 0.04 between 200 and $800 \text{ }^\circ\text{C}$. However, the absolute value of the emissivity obtained with this model is at least two times lower than the measured. After a correction of its absolute value this model could be used to extrapolate the emissivity values at higher temperature. It is important to stress that the emissivity measurement did not present any hysteresis, confirming that under the vacuum conditions in the range of 10^{-5} Pa no surface modification (particularly potential surface oxidation) have been induced during the temperature excursions. To confirm that, every measurement campaign has been performed at least two times and measurements have been done during temperature ramp up and ramp down. However, a first heating phase (about 5h outgazing at $800 \text{ }^\circ\text{C}$) was necessary to clean the sample surface from any residuals from the machining process or handling. Raman spectroscopy, which is sensitive to chemical bonds, was performed on all samples. The set up used is a Horiba Jobin Yvon HR800 set up, 600 grooves/mm grating, 514 nm laser, with spectra recorded in 10 seconds with a $100\times$ objective, with a power density of $\approx 0.6 \text{ mW}/\mu\text{m}^2$. The analysis performed on all samples was not able to detect W-O bonds, which are in general very intense [31].

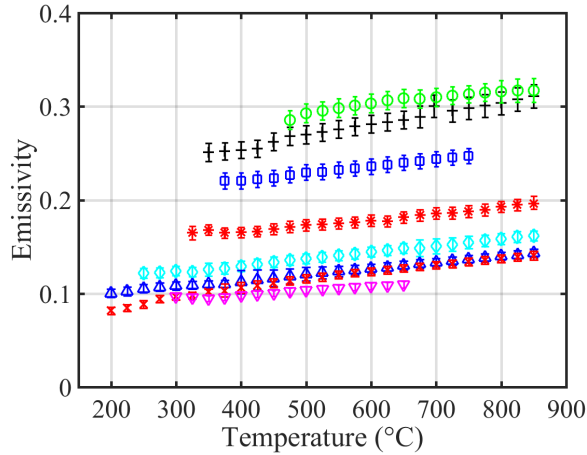


Figure 4. Emissivity of W bulk as function of the temperature for the 8 filters: \circ 1.7 μm , \square 2.14 μm , $*$ 2.6 μm , \diamond 3.255 μm , \blacktriangle 3.9 μm (STD), \times 4.35 μm (WA), \blacktriangledown 4.75 μm and $+$ 1.6-2.1 μm (VHR).

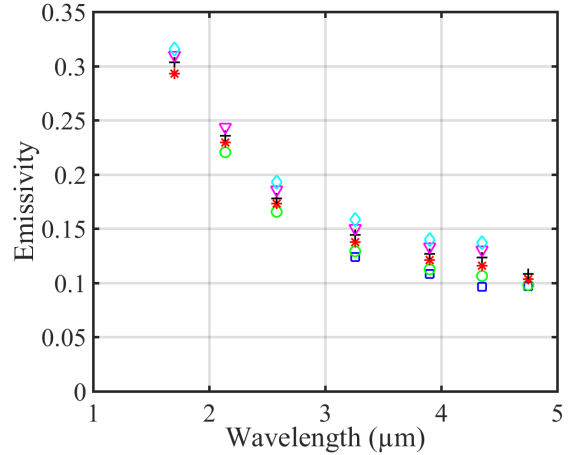


Figure 5. Emissivity of W bulk as function of the wavelength for several temperature: \square 300 $^{\circ}\text{C}$, \circ 400 $^{\circ}\text{C}$, $*$ 500 $^{\circ}\text{C}$, $+$ 600 $^{\circ}\text{C}$, \blacktriangledown 700 $^{\circ}\text{C}$, \diamond 800 $^{\circ}\text{C}$.

4.2. W coating

Figure 6 shows the W coating emissivity dependences with the temperature and wavelength. The temperature range is lower than the W bulk, up to 550 $^{\circ}\text{C}$ contrary to 850 $^{\circ}\text{C}$ previously, due to the lower efficiency of the electron bombardment with the graphite underneath (electrical conductivity of the graphite being lower than metals). Nevertheless, we can observe the same dependencies on temperature and wavelength as for the W bulk. Once again, although the emissivity is lower at high wavelength, the accessible experimental temperature range toward low temperatures remains larger.

Figure 7 shows a comparison of the measured emissivities for the W bulk and coating as function of the wavelength at 500 $^{\circ}\text{C}$. We can clearly see the same wavelength dependence with slightly higher emissivity for the W coating (between 10 to 30 % higher than W bulk). The W coating has been deposited on the graphite by physical vapor deposition. Glow discharge optical emission spectroscopy performed on the W coating has shown the low impurity content of the coating (< 5 %) [28]. This is well in line with the observations made that the W coating emissivity behaves like the W bulk emissivity. The higher W coating emissivity could be explained by the higher roughness of the W coating with $R_a \approx 2 \mu\text{m}$ in comparison to $R_a \approx 1.2 \mu\text{m}$ for W bulk.

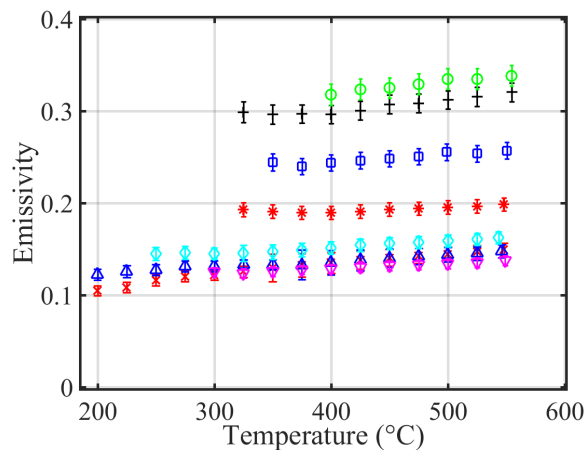


Figure 6. Emissivity of W coating as function of the temperature for the 8 filters: \circ 1.7 μm , \square 2.14 μm , $*$ 2.6 μm , \diamond 3.255 μm , \blacktriangle 3.9 μm (STD), \times 4.35 μm

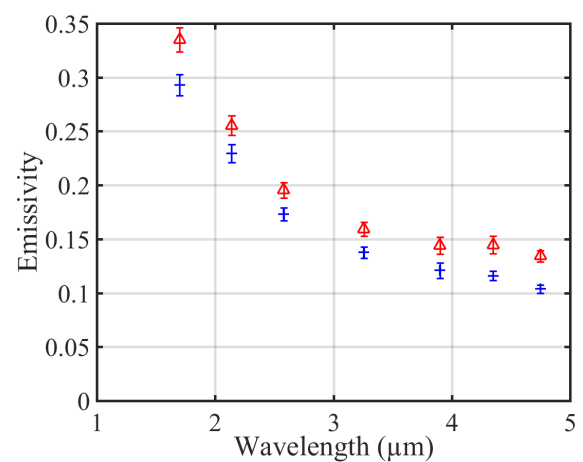


Figure 7. Emissivity as function of the wavelength at 500 $^{\circ}\text{C}$ for the (+) W bulk and (\blacktriangle) W coating.

(WA), ▼ 4.75 μm and + 1.6-2.1 μm (VHR).

4.3. W damaged samples

The whole W bulk samples available, provided four different surface states. A “healthy” surface corresponding to the W bulk with the same surface as the ITER-like PFC in WEST with $R_a \approx 1.12 \mu\text{m}$; a polished surface with $R_a \approx 0.1 \mu\text{m}$; a low damaged area with small cracks and $R_a \approx 0.42 \mu\text{m}$ and finally a moderately damaged area with cracks networks and $R_a \approx 1.39 \mu\text{m}$. The roughness has been measured by chromatic confocal microscopy [32].

Figure 8 shows the resulting emissivities as function of the temperature with the VHR filter (1.6 to 2.1 μm), the one which is used to monitor the pre-damaged component in WEST, for the different W samples. We can observe that the temperature dependence is the same for all surface state, the emissivity increasing by about 0.04-0.06 from 400 to 800 $^{\circ}\text{C}$. However, the absolute value is clearly different for each sample. As expected, the polished area exhibits the lowest emissivity of 0.2. The next level of emissivity is for the healthy sample, presented in the section 3.1, with an emissivity of 0.3. And finally, also as expected, the emissivity increases with the damages with an emissivity of 0.5 and 0.6 respectively for low and moderate damage.

The emissivity of the four surfaces states cannot be ranked by consideration of the R_a parameter only. The type of roughness (uniform, machining with grooves or cracks) being also important and not always “reflected” by the R_a parameter. The small crack seems to have a huge influence on the emissivity, higher than the machining roughness of the W bulk. The crack width is equivalent to the wavelength studied here, few μm , and they seem to be small trap for the infrared radiation acting as small blackbody giving a high effective emissivity at the mm scale.

The emissivities of the damaged areas have been also measured for the two others WEST filters. Figure 9 shows the emissivity ratio between the damaged area and the healthy surface for the three WEST filters. We can observe that the ratio has a small temperature dependence and once again the main dependence is for the wavelength with ratio about 3.5 for the STD and WA filter in the case of the damage #2. All the measurements have been summarized in the appendix tables.

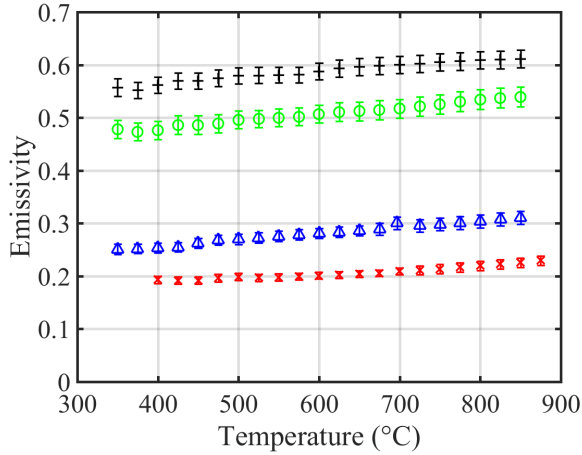


Figure 8. Emissivity as function of the temperature with VHR filter (1.6-2.1 μm) for the (▲) W healthy, (×) W polished, (○) W damage #1 and (+) W damage #2.

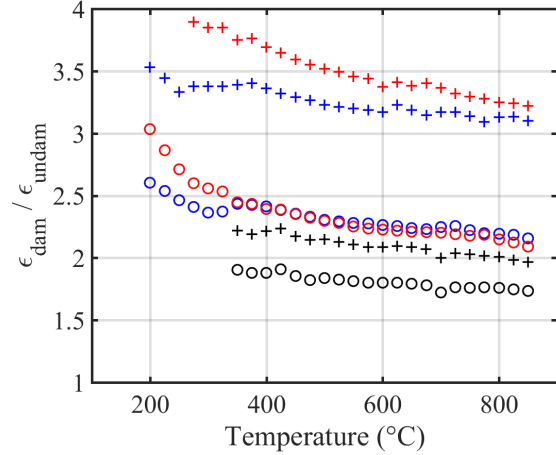


Figure 9. Emissivity ratio damaged over undamaged W sample for the two damages (○) #1 (+) #2 as function of the temperature for the 3 WEST filters: 1.6-2.1 μm (VHR), 3.9 μm (STD) and 4.35 μm (WA).

5. Summary

A dedicated experimental setup has been developed to measure the emissivity of materials as a function of temperature and wavelength. The study has been performed with W samples corresponding to the plasma facing component of the WEST divertor which are ITER relevant in case of bulk samples. The temperature domain investigated varies from 200 to 850 °C whilst the wavelength range extends from 1.7 to 4.75 μm. The three IR interference filters used in WEST have been used to give direct value of the surface emissivity for the IR monitoring and protection of plasma facing components during WEST experiment. The experimental results show that the tungsten emissivity varies by about a factor of three from 0.1 to 0.3 for wavelength at 4.75 and 1.7 μm, respectively. The effect of the temperature on the emissivity exhibits a lower dependence with an increase of 0.04 from 200 to 850 °C for all the wavelengths studied in the 1.7 to 4.75 μm range.

Throughout this study, the surface state shows a strong influence on the experimental results with a large increase of the emissivity with the micro crack and cracks network presence. Indeed, an increase by of a factor between 2 and 4, depending on the damaged level and wavelength, has been measured. These damage levels obtained with fast transient heat load mimicking the fast transient called ELMs, for Edge Localized Modes, will be likely dominant in the process of plasma surface interaction on the ITER divertor. This study also highlights the inadequacy of the use of the roughness parameter Ra only, to explain the emissivity behavior as a function of the roughness. All these measurements will be used for consolidating the WEST PFC safety strategy and contribute to the determination of the absolute surface temperature by IR thermography allowing also physics studies related to the plasma heat load pattern (width and intensity).

Acknowledgments

This work has been carried out within the framework of the EUROfusion Consortium and has received funding from the Euratom research and training programme 2014–2018 and 2019-2020 under grant agreement No 633053. The views and opinions expressed herein do not necessarily reflect those of the European Commission and ITER Organization.

References

- [1] R.A. Pitts et al., *Journal of Nuclear Materials* 438 (2013) S48-S56
- [2] R.A. Pitts et al., *Nuclear Materials and Energy* 12 (2017) 60-74
- [3] T. Hirai et al., *Fusion Engineering and Design* 125 (2017) 250-255
- [4] J. Bucalossi et al., *Fusion Engineering and Design* 89 (2014) 907-912
- [5] C. Bourdelle et al., *Nuclear Fusion* 55 (2015) 063017
- [6] X. Courtois et al., *Fusion Engineering and Design* 136 (2018) 1499-1504
- [7] P. Moreau et al., *Fusion Engineering and Design* 123 (2017) 1029-1032
- [8] L. Letellier et al., *Fusion Engineering and Design* 123 (2017) 650-653
- [9] N. Yoshida, *Journal of Nuclear Materials* 266-269 (1999) 197-206
- [10] T. Hirai et al., *Nuclear Materials and Energy* 9 (2016) 616-622
- [11] M. Kocan et al., *Physica Scripta*, (2016) T167
- [12] M.-H. Aumeunier et al., *Nuclear Materials and Energy* 12 (2017) 1265-1269
- [13] W.E. Forsythe and A.G. Worthing, *Astrophysical Journal* 61 (1925) 146
- [14] J.C. De Vos, *Physica* Volume 20, Issue 7, (1954) 690-714.
- [15] L.D. Larrabee, *Massachusetts Institute of Technology*, May 1957
- [16] Y.S. Touloukian and D.P. Dewitt, *Thermophysical properties of matter* 7 (1970) 776-791
- [17] J.H. Weaver et al., *Physical Review B* 12 (1975) 1293-7
- [18] M.A. Ordal et al., *Applied Optics* 24 (1985) 4493-4499
- [19] T. Matsumoto et al., *International Journal of Thermophysics* 20 (1999) 943-952
- [20] H. Bolt et al., *Journal of Nuclear Materials* 307-311 (2002) 43-52
- [21] C. Cagran et al., *International Journal of Thermophysics* 26 (2005) 1001-1015
- [22] F. Lott et al., *Fusion Engineering and Design* 85 (2010) 146-152

- [23] E. Brodu et al., *Acta Materialia* 84 (2015) 305-316
- [24] C. Ruset et al., *Fusion Engineering and Design* 114 (2017) 192-195
- [25] M. Minissale et al., *Journal of Physics D: Applied Physics* 50 (2017) 455601
- [26] D. Guilhem et al., *Physica Scripta T167* (2016) 014066
- [27] M. Firdaouss et al., *Fusion Engineering and design* 124 (2017) 207-210
- [28] M. Houry et al., <https://doi.org/10.1016/j.fusengdes.2019.02.017>
- [29] Th. Loewenhoff et al., *Fusion Engineering and Design* 87 (2012) 1201-1205
- [30] M.A. Bramson, *Infrared radiation a handbook for application, Optical Physics and Engineering*, (1968)
- [31] Y. Addab et al., *Physica Scripta T167* (2016) 014036
- [32] E. Gauthier et al., *Journal of Nuclear Materials* 538 (2013) S1216-1220

Appendix

| Sample | Temperature | | | | | | | | | | | | | |
|-------------|---------------------------------|----------------------|----------------------|----------------------|----------------------|----------------------|----------------------|----------------------|----------------------|----------------------|----------------------|----------------------|----------------------|----------------------|
| | 200°C | 225°C | 250°C | 275°C | 300°C | 325°C | 350°C | 375°C | 400°C | 425°C | 450°C | 475°C | 500°C | |
| | $\lambda=1.7\pm 0.1\mu\text{m}$ | | | | | | | | | | | | | |
| W bulk | | | | | | | | | | | | 0.285 ± 0.01 | 0.293 ± 0.01 | |
| W coating | | | | | | | | | 0.318 ± 0.012 | 0.323 ± 0.011 | 0.325 ± 0.011 | 0.329 ± 0.011 | 0.335 ± 0.011 | |
| W damage #1 | | | | | | | | 0.488 ± 0.019 | 0.483 ± 0.017 | 0.482 ± 0.017 | 0.486 ± 0.017 | 0.488 ± 0.017 | 0.49 ± 0.016 | |
| W damage #2 | | | | | | | 0.531 ± 0.02 | 0.537 ± 0.018 | 0.541 ± 0.017 | 0.542 ± 0.017 | 0.55 ± 0.017 | 0.548 ± 0.016 | 0.552 ± 0.016 | |
| W polished | | | | | | | | | 0.241 ± 0.011 | 0.24 ± 0.01 | 0.24 ± 0.009 | 0.238 ± 0.009 | 0.241 ± 0.009 | |
| | | | | | | | | | | | | | | |
| | Temperature | | | | | | | | | | | | | |
| | 525°C | 550°C | 575°C | 600°C | 625°C | 650°C | 675°C | 700°C | 725°C | 750°C | 775°C | 800°C | 825°C | 850°C |
| | $\lambda=1.7\pm 0.1\mu\text{m}$ | | | | | | | | | | | | | |
| W bulk | 0.295 ± 0.01 | 0.298 ± 0.01 | 0.301 ± 0.01 | 0.303 ± 0.01 | 0.307 ± 0.01 | 0.309 ± 0.01 | 0.308 ± 0.01 | 0.31 ± 0.009 | 0.312 ± 0.009 | 0.313 ± 0.009 | 0.315 ± 0.009 | 0.316 ± 0.012 | 0.317 ± 0.012 | 0.317 ± 0.013 |
| W coating | 0.335 ± 0.011 | 0.338 ± 0.011 | | | | | | | | | | | | |
| W damage #1 | 0.49 ± 0.016 | 0.487 ± 0.016 | 0.49 ± 0.016 | 0.49 ± 0.016 | 0.486 ± 0.016 | 0.488 ± 0.016 | 0.49 ± 0.016 | 0.491 ± 0.016 | 0.493 ± 0.015 | 0.495 ± 0.02 | 0.496 ± 0.02 | 0.497 ± 0.02 | 0.5 ± 0.021 | 0.502 ± 0.021 |
| W damage #2 | 0.551 ± 0.016 | 0.553 ± 0.015 | 0.556 ± 0.015 | 0.551 ± 0.015 | 0.553 ± 0.015 | 0.556 ± 0.015 | 0.558 ± 0.015 | 0.559 ± 0.015 | 0.566 ± 0.018 | 0.567 ± 0.019 | 0.569 ± 0.02 | 0.571 ± 0.02 | 0.574 ± 0.021 | 0.577 ± 0.022 |
| W polished | 0.238 ± 0.009 | 0.232 ± 0.008 | 0.231 ± 0.008 | 0.229 ± 0.007 | 0.232 ± 0.007 | 0.232 ± 0.007 | 0.232 ± 0.007 | 0.23 ± 0.007 | 0.23 ± 0.007 | 0.232 ± 0.007 | 0.233 ± 0.007 | 0.234 ± 0.007 | 0.236 ± 0.008 | 0.237 ± 0.008 |
| | | | | | | | | | | | | | | |

Table A.1. Emissivity measurement for all samples at $1.7\mu\text{m}$

| Sample | Temperature | | | | | | | | | | | | | |
|---|-----------------------------------|----------------------|----------------------|----------------------|----------------------|----------------------|----------------------|----------------------|----------------------|----------------------|----------------------|----------------------|----------------------|----------------------|
| | 200°C | 225°C | 250°C | 275°C | 300°C | 325°C | 350°C | 375°C | 400°C | 425°C | 450°C | 475°C | 500°C | |
| | $\lambda=2.14\pm 0.05\mu\text{m}$ | | | | | | | | | | | | | |
| W bulk | | | | | | | | 0.221 ± 0.009 | 0.22 ± 0.009 | 0.222 ± 0.009 | 0.223 ± 0.009 | 0.227 ± 0.008 | 0.229 ± 0.008 | |
| W coating | | | | | | | 0.244 ± 0.009 | 0.24 ± 0.009 | 0.243 ± 0.009 | 0.246 ± 0.009 | 0.248 ± 0.009 | 0.25 ± 0.009 | 0.255 ± 0.009 | |
| | | | | | | | | | | | | | | |
| | Temperature | | | | | | | | | | | | | |
| | 525°C | 550°C | 575°C | 600°C | 625°C | 650°C | 675°C | 700°C | 725°C | 750°C | 775°C | 800°C | 825°C | 850°C |
| | $\lambda=2.14\pm 0.05\mu\text{m}$ | | | | | | | | | | | | | |
| W bulk | 0.23 ± 0.008 | 0.232 ± 0.008 | 0.234 ± 0.008 | 0.236 ± 0.008 | 0.238 ± 0.008 | 0.24 ± 0.008 | 0.242 ± 0.008 | 0.244 ± 0.008 | 0.245 ± 0.008 | 0.247 ± 0.008 | | | | |
| W coating | 0.254 ± 0.009 | 0.257 ± 0.009 | | | | | | | | | | | | |
| | | | | | | | | | | | | | | |
| | Temperature | | | | | | | | | | | | | |
| | 200°C | 225°C | 250°C | 275°C | 300°C | 325°C | 350°C | 375°C | 400°C | 425°C | 450°C | 475°C | 500°C | |
| | $\lambda=2.6\pm 0.05\mu\text{m}$ | | | | | | | | | | | | | |
| W bulk | | | | | | | 0.165 ± 0.007 | 0.168 ± 0.006 | 0.165 ± 0.006 | 0.165 ± 0.006 | 0.166 ± 0.006 | 0.169 ± 0.006 | 0.171 ± 0.006 | 0.173 ± 0.006 |
| W coating | | | | | | | 0.193 ± 0.008 | 0.191 ± 0.007 | 0.19 ± 0.007 | 0.19 ± 0.007 | 0.191 ± 0.007 | 0.193 ± 0.007 | 0.194 ± 0.007 | 0.195 ± 0.007 |
| | | | | | | | | | | | | | | |
| | Temperature | | | | | | | | | | | | | |
| | 525°C | 550°C | 575°C | 600°C | 625°C | 650°C | 675°C | 700°C | 725°C | 750°C | 775°C | 800°C | 825°C | 850°C |
| | $\lambda=2.6\pm 0.05\mu\text{m}$ | | | | | | | | | | | | | |
| W bulk | 0.174 ± 0.006 | 0.175 ± 0.006 | 0.176 ± 0.006 | 0.178 ± 0.006 | 0.177 ± 0.006 | 0.182 ± 0.006 | 0.184 ± 0.006 | 0.186 ± 0.006 | 0.186 ± 0.006 | 0.188 ± 0.006 | 0.189 ± 0.006 | 0.193 ± 0.006 | 0.195 ± 0.006 | 0.196 ± 0.006 |
| W coating | 0.196 ± 0.007 | 0.198 ± 0.007 | | | | | | | | | | | | |
| | | | | | | | | | | | | | | |
| Table A.2. Emissivity measurement for W bulk and coating at 2.14 and 2.6 μm | | | | | | | | | | | | | | |